



Pharmaceutics, Drug Delivery and Pharmaceutical Technology

## Incomplete Loading of Sodium Lauryl Sulfate and Fasted State Simulated Intestinal Fluid Micelles Within the Diffusion Layers of Dispersed Drug Particles During Dissolution



Kendra Galipeau\*, Michael Socki, Adam Socia, Paul A. Harmon\*

Analytical Sciences, Merck Research Laboratories, Merck &amp; Company, Inc., West Point, Pennsylvania 19486

## ARTICLE INFO

## Article history:

Received 6 March 2017

Revised 8 June 2017

Accepted 8 June 2017

Available online 15 June 2017

## Keywords:

micelle  
nanoparticles  
solubility  
dissolution rate  
surfactant

## ABSTRACT

Poorly water soluble drug candidates have been common in developmental pipelines over the last several decades. This has fueled considerable research around understanding how bile salt and model micelles can improve drug particle dissolution rates and human drug exposure levels. However, in the pharmaceutical context only a single mechanism of how micelles load solute has been assumed, that being the direct loading mechanism put forth by Cussler and coworkers (Am Inst Chem Eng J. 1976;22(6):1006–1012) 40 years ago. In this model, micelles load at the particle surface and will be loaded to their equilibrium loading values. More recently, Kumar and Gandhi and coworkers (Langmuir. 2003;19:4014–4026) developed a comprehensive theory of micelle solubilization which also features an indirect loading mechanism which they argue should operate in ionic surfactant systems. In this mechanism, micelles cannot directly load at the solute particle surface and thus may not reach equilibrium loading values within the particle diffusion layer. In this work, we endeavor to understand if the indirect micelle loading mechanism represents a plausible description in the pharmaceutical context. The overall data in SLS and FaSSIF systems obtained here, as well as several other previously published datasets, can be described by the indirect micelle loading mechanism. Implications for pharmaceutical development of poorly soluble compounds are discussed.

© 2018 Published by Elsevier Inc. on behalf of the American Pharmacists Association.

## Introduction

The increasing prevalence of poorly water soluble compounds in pharmaceutical development pipelines over the last several decades has been repeatedly noted in the literature.<sup>1–3</sup> Fortunately, equilibrium solubility values of such drug candidates are often increased significantly in fasted state simulated intestinal fluid (FaSSIF) due to the presence of bile salt micelles. This has led to a large body of work around measuring, understanding, and modeling expected drug particle dissolution rate improvements due to solubilization by micelles.<sup>4–20</sup> The expected increases in low solubility drug particle dissolution rates from micelles have further been incorporated into overall computational oral absorption models<sup>10,13,16,21,22</sup> which attempt to more quantitatively capture the impact that drug-loaded

micelles will have on the fraction of the oral dose which can be absorbed. In all of this work, it has been assumed that micelles will be fully loaded to their saturated equilibrium solubility values within the diffusion layers of the drug particles during dissolution in the micellar media. This assumption allows the use of a modified Nernst-Brunner model to describe the micelle contributions to the dissolution rate.<sup>23–25</sup> This simple approach has found widespread acceptance.

The assumption of fully loaded micelles is also supported by early work on solubilization by Cussler and coworkers.<sup>4,15</sup> Cussler and coworkers studied the solubilization of long-chain fatty acid particles (e.g., lauric, palmitic, and stearic acid) by surfactant solutions such as sodium lauryl sulfate (SLS) and sodium taurocholate (NaTC). These solutes were considered insoluble in the aqueous (buffer) phase. Figure 1a describes the general Cussler mechanism as adapted from his work. The salient feature in Figure 1a is that Cussler and coworkers argued that the fatty acid molecules are incorporated into the micelles directly at the solid acid particle surface.<sup>13</sup> This direct loading mechanism is interpreted to produce SLS or NaTC micelles which are fully loaded to their saturated equilibrium solubility values prior to micelle desorption from the surface and diffusion to bulk solution.

Current address for Harmon: PharRxmon Consulting, Eagleville, Pennsylvania 19408.

\* Correspondence to: Kendra Galipeau (Telephone: 215-652-1552; Fax: 215-652-2835) and Paul A. Harmon (Telephone: 610-212-9817; Fax: 215-652-2835).

E-mail addresses: [kendra.kathan@merck.com](mailto:kendra.kathan@merck.com) (K. Galipeau), [pharxmonconsulting@comcast.net](mailto:pharxmonconsulting@comcast.net) (P.A. Harmon).

## Nomenclature

$A$	surface area of the particle
$\beta_0$	surface kinetic coefficient
$\beta_{01}$	surface kinetic coefficient in blank buffer solution
$C_b$	concentration in bulk solution
$C_s$	saturated equilibrium solubility in buffer
CMC	critical micelle concentration
$C_T$	saturated equilibrium solubility in the micellar system
$D_a$	Damkohler number for the buffer phase
$D_{am}$	Damkohler number for the micellar phase
$D_{eff}$	effective diffusion coefficient
$D_{micelle}$	diffusion coefficient of micelles
$D_{mol}$	diffusion coefficient of drug molecules
$d_m$	diameter of micelles
$\delta$	diffusion layer thickness
$f_{mol}$	fraction of the total solubilized drug in the buffer,
	$f_{mol} = \frac{C_s}{C_T}$
$f_{micelle}$	fraction of the total solubilized drug in the micelles,
	$f_{micelle} = \frac{C_T - C_s}{C_T}$

$k$	Boltzmann constant
$K_{eq}$	[concentration of drug in the micelles (per unit volume of micelle)]/[concentration in the buffer phase (per unit volume of buffer phase)]
$k_s$	interfacial reaction rate constant
$m$	mass
$M_{Uj}$	amount of undissolved drug
$M_{Dt}$	total dissolved amount of drug
MW	molecular weight
$\eta$	viscosity
$\emptyset$	volume fraction of micelles
$\rho$	density
$p$	dimensionless parameter which scales the micellar contribution to mass transport
$r$	radius of the particle
$r_0$	initial radius of the particle
$T$	absolute temperature
$T_{infin}$	time to infinite dissolution
$\gamma$	dimensionless constant
$V$	volume of dissolution media

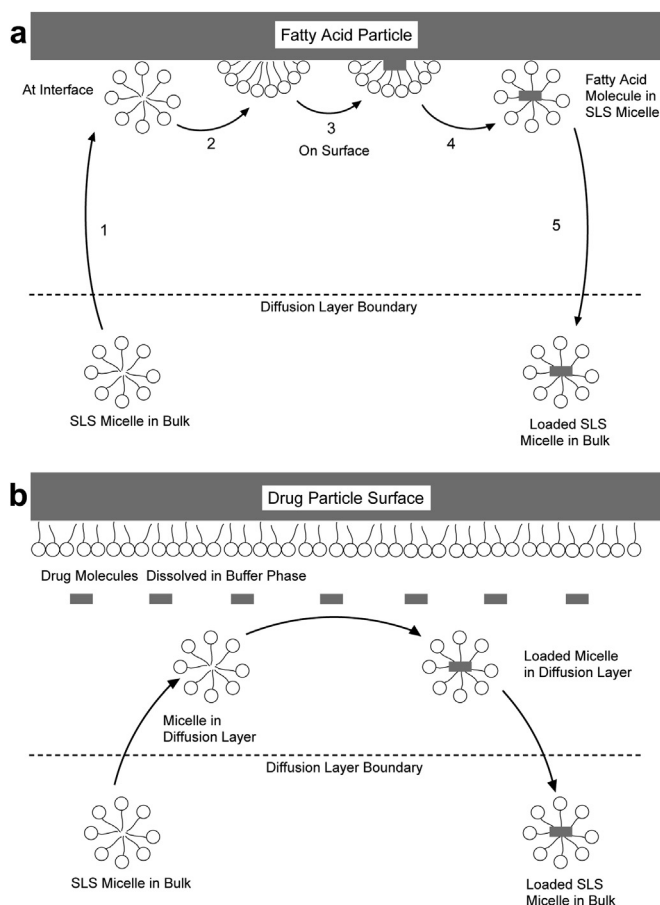


**Figure 1.** (a) Cussler's 5-step direct loading mechanism (depicted here for SLS): (1) diffusion of SLS micelle from bulk to the interface; (2) adsorption onto the surface of the fatty acid particle; (3) incorporation of fatty acid molecule into the SLS micelle on the surface of the fatty acid particle; (4) desorption of loaded micelle; and (5) diffusion of loaded micelle to bulk. (b) Kumar and Gandhi's indirect loading mechanism for ionic surfactants such as SLS. Ionic repulsion prohibits contact of micelle with drug particle surface. Drug loads into micelle by diffusional contact with dissolved drug molecules.

Almost 30 years later, Kumar and Gandhi and coworkers<sup>5</sup> developed a more comprehensive treatment of solubilization by surfactant systems. In their model, the direct loading mechanism in Figure 1a will only be possible in non-ionic surfactant systems. The primary focus of their efforts was to quantitatively describe micelle loading in ionic surfactant systems such as SLS and NaTC (as well as FaSSIF by analogy). The resulting indirect loading mechanism is depicted in Figure 1b. This mechanism does not allow for direct contact of micelles with the solid particle surface, due to charge-charge repulsion from monomer surfactant molecules coating the hydrophobic drug particle surface and the similarly charged micelles (consider SLS as an example as shown in Fig. 1b). Solute molecules dissolve only directly into the buffer phase, and in parallel, micelles can take up solute molecules from the buffer phase near the dissolving particle surface and diffuse to bulk solution to assist in the mass transport. Sailaja et al. demonstrated that the indirect model could quantitatively describe benzene, decane,<sup>5,9,10</sup> and Cussler's fatty acid particle dissolution in SLS solutions (in the latter case, by explicitly considering the non-zero fatty acid solubility values). Subsequently, Ariyaprakai and Dungan<sup>26-28</sup> studied *n*-hexadecane, *n*-tetradecane, and *n*-dodecane droplets in both SLS and the non-ionic surfactant Tween 20 and varied the viscosity of the medium. This allowed them to observe whether the diffusion of solute molecules was involved in the rate-limiting steps of the dissolution process. In Tween 20, they found that both direct and indirect micelle loading contributed to the dissolution of the least soluble compounds. In the case of ionic SLS, however, the dissolution process of all 3 solutes was found to be dominated by the indirect micelle loading mechanism, in agreement with Kumar and Gandhi's solubilization model.

Despite these later validations of ionic surfactants exhibiting indirect micelle loading in Figure 1b, the direct micelle loading concept in Figure 1a appears to have remained embedded within the pharmaceutical literature. If drug particles always exhibited the dissolution enhancements expected from fully loaded micelles and Nernst-Brunner assumptions, then the differentiation between the mechanisms in Figures 1a and 1b would be academic. However, recently several reports<sup>8,29</sup> have demonstrated much slower drug particle dissolution rates than expected (all these studies were carried out in ionic surfactants such as SLS, NaTC, or FaSSIF). Shekunov<sup>29</sup> argues that such slow dissolution rates of poorly soluble drug

particles may in fact be typical, rather than the exception. The results have been interpreted in the context of Figure 1a. The slow dissolution rates then must be attributed to slow, rate-limiting steps involving formation/desorption of fully loaded micelles at the drug particle surface.<sup>7,8,12,13,15,18,29</sup> This leads to concerns about the predictability of such dissolution slowing, as it is not readily obvious from consideration of the material properties of the surfactant and the drug when this should be a rate-limiting step. Such processes will also limit the dissolution rate enhancement that can be expected with drug particle size reduction.<sup>8,29</sup> These issues pose challenges for the development and optimization of poorly soluble drug formulations.

In this work, we endeavor to examine slower drug particle dissolution rates for the first time in the context of Figure 1b. The key feature of Kumar and Gandhi's indirect loading model is that the  $K_{eq}$  value between the micellar and buffer phases will control whether micelles will be able to reach equilibrium loading values within solute particle diffusion layers. Thus drugs with increasingly large  $K_{eq}$  values will suffer from slower mass transport compared to fully loaded micelle assumptions. We examine 4 drug particle populations with a wide range of  $K_{eq}$  in the ionic surfactants SLS and FaSSIF. We also examine previous work by Sugano and coworkers<sup>13</sup> and Williams and Johnston and coworkers.<sup>8</sup> The results are found to be consistent with Kumar and Gandhi's predictions and the indirect loading mechanism in Figure 1b. This leads to a significantly different view of the predictability of this type of drug particle dissolution slowing. Finally, in the context of Figure 1b, a view of expected dissolution rate enhancements from poorly soluble drug particle size reduction in micellar media is developed. This view suggests that poorly soluble drug nanoparticles will often be controlled by dissolution of the drug into the buffer phase alone, with micelles playing no role in the mass transfer.

## Theory

### Modeling Drug Particle Dissolution in the Presence of Micelles-Equilibrated Micelles

The Nernst-Brunner approximation<sup>23,24</sup> to drug particle dissolution has been commonly used and assumes that the solubility limit of the drug will be reached in a thin layer at the surface of the particle quickly, compared to the subsequent diffusion of the dissolved drug across the particle's diffusion layer to the bulk solution. Figure 2 depicts the assumed conditions. In this limit, the mass ( $m$ ) change of the particle due to dissolution is given as follows:

$$\frac{dm}{dt} = \frac{D_{mol}}{\delta} A (C_s - C_b) \quad (1)$$

where  $D_{mol}$  is the drug molecule diffusion coefficient,  $\delta$  the diffusion layer thickness,  $A$  the surface area of the particle,  $C_s$  the saturated equilibrium solubility in buffer, and  $C_b$  the concentration in bulk solution. The Nernst-Brunner equation has been modified by Johnson<sup>9,21</sup> and later Sugano and coworkers<sup>13</sup> to account for polydisperse particle size populations. Several groups<sup>5,12,14,16,18</sup> have additionally modified the Nernst-Brunner theory to account for the contribution to the dissolution rate of the particle by micelles by introducing an effective diffusion coefficient, ( $D_{eff}$ , Eq. 2) which is simply a population weighted average of the solute molecule's diffusion coefficient and the diffusion coefficient of the micelle:

$$D_{eff} = D_{mol}f_{mol} + D_{micelle}f_{micelle} \quad (2)$$

where  $f_{mol}$  and  $f_{micelle}$  are the fraction of the total solubilized drug in the buffer or in the micelles, respectively (measured in a saturated

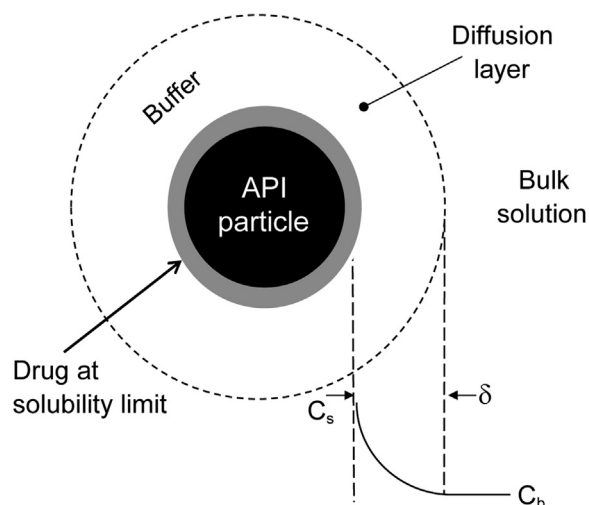


Figure 2. Schematic of diffusion-controlled drug particle dissolution described by Nernst-Brunner assumptions.

micellar solution of the solute);  $f_{mol} = \frac{C_s}{C_T}$ ;  $f_{micelle} = \frac{C_T - C_s}{C_T}$ ; and  $D_{mol}$  and  $D_{micelle}$  the diffusion coefficients of the drug molecule and the micelle, respectively (the diffusion coefficient of drug-bound micelles can vary from free micelles<sup>7</sup>; however, this difference is often small enough that the diffusion of drug-bound micelles can be approximated as the diffusivity of the micelles<sup>4,12,13</sup> and that approach is adopted here). Equation 2 thus assumes the micelles are fully equilibrated (loaded) within the solute particle diffusion layer. This approach is consistent with the direct loading mechanism of Cussler described in Figure 1a, and allows a straightforward mathematical treatment for the contribution of micelles to particle dissolution rates.

The commercially available DDDPlus™ program is used to model the dispersed drug particle dissolution profiles with the Nernst-Brunner model option. The drug particle size distributions are measured separately (see Methods) and imported into the DDDPlus™ program; a discrete number of bins is used to represent the entire curve and the dissolution is calculated at each bin. The values of  $D_{eff}$  are calculated as in Equation 2 from the solubility limit data and entered into the DDDPlus™ program for the diffusion coefficient. The form of the Nernst-Brunner equation that is effectively used is then given as follows:

$$\frac{dM_{Ui}}{dt} = - \left[ \frac{3D_{eff}\gamma}{\delta_i r_i \rho} \right] \left( C_T - \frac{M_{Dt}}{V} \right) M_{Ui} \quad (3)$$

where the subscript  $i$  refers to the particular particle bin and  $M_{Ui}$  the amount of undissolved drug (mg),  $D_{eff}$  the diffusion coefficient ( $\text{cm}^2/\text{s}$ , as defined in Eq. 2),  $\gamma$  the dimensionless constant,  $\delta_i$  the diffusion layer thickness (cm),  $r_i$  the particle radius (cm),  $\rho$  the density of the drug particles (mg/mL),  $M_{Dt}$  the total dissolved amount of drug (mg),  $V$  the volume of dissolution media (mL), and  $C_T$  the saturated equilibrium solubility in the micellar system (mg/mL).

The DDDPlus™ program assumes that the diffusion layer thickness is equal to the particle diameter up to a diameter of 30  $\mu\text{m}$ , beyond which the diffusion layer thickness remains 30  $\mu\text{m}$ . The program adjusts the diffusion layer thickness of all particles over the course of the simulation to reflect the dissolving particle's radius. Simultaneously, the program accounts for the solubility gap term ( $C_T - M_{Dt}/V$ ) in Equation 3 which drives the dissolution process. As described in Methods, the amount of drug particles added to the micellar solution is limited to prevent the solubility gap term in Equation 3 from rapidly approaching zero.

### Modeling Drug Particle Dissolution in the Presence of Micelles—Indirect Micelle Loading

The Kumar and Gandhi model for micelle loading in ionic surfactants (Fig. 1b) assumes that micelles cannot come into direct contact with the drug particle surface due to charge-charge repulsions from adsorbed surfactant monomers on the particle surface and the similarly charged micelles. Micelles only enhance dissolution rates by picking up drug molecules dissolved in the buffer phase near the drug particle surface and then diffusing to bulk solution. Although it is not our intent to recount all the details of the theory described by Kumar and Gandhi and coworkers,<sup>5</sup> it is important that the reader fully appreciates the key role that the equilibrium partition coefficient between the micellar phase and the buffer phase ( $K_{eq}$ ) plays in determining whether micelles can be expected to be fully or only partially loaded (with respect to their equilibrium saturated solution values) within dissolving drug particle diffusion layers.  $K_{eq}$  is defined as follows:

$$K_{eq} = \frac{\text{[concentration of drug in the micelles (per unit volume of micelle)]}}{\text{[concentration in the buffer phase (per unit volume of buffer phase)]}} \quad (4)$$

This critical aspect of the indirect loading model can be appreciated from considering Figures 1b and 2. Assume a 10 micron drug particle and an SLS micelle solution. The diffusional pathways of the micelles are fixed; the empty micelles enter the particle diffusion layer and diffuse into the blue region of drug saturated buffer solution near the particle surface (Fig. 2) and out through the 10 micron diffusion layer to bulk solution (no direct contact with particle surface). In case 1, suppose the drug has a very high  $K_{eq}$  value, due to several drug molecules needed per micelle at saturation, as well as the drug having a very low buffer solubility value (e.g., tens of ng/mL). In this case, there are simply not nearly enough diffusional encounters between the micelle and dissolved drug molecules to load the micelle to its equilibrium saturated value before exiting the particle diffusion layer. Consider case 2, in which the drug  $K_{eq}$  value is much more modest due to a smaller number of drug molecules found in the micelle at saturation as well as a much higher buffer solubility value (tens of  $\mu\text{g/mL}$ ). In case 2, the same diffusional pathway taken by the SLS micelle in case 1 leads to many more encounters with dissolved drug in the buffer phase. In case 2, the micelle can load to the equilibrium saturated value prior to exit from the particle diffusion layer.

Kumar and Gandhi and coworkers<sup>5</sup> apply Damkohler numbers for the micellar phase and the buffer phase to more quantitatively understand the interplay of drug particle size, micelle size, and  $K_{eq}$  values on the degree of micelle loading which can be expected within particle diffusion layers. For a given drug particle size and surfactant system, the Damkohler number for the micellar phase,  $D_{am}$ , is the key parameter which predicts the degree of micellar loading.  $D_{am}$  relates the rate at which micelles load with drug to the rate at which micelles carry the drug away.  $D_{am}$  is inversely proportional to the  $K_{eq}$  value and is defined as follows:

$$D_{am} = \frac{12r^2D_{mol}}{d_m^2K_{eq}D_{micelle}} \quad (5)$$

where  $d_m$  is the diameter of micelles,  $D_{micelle}$  the diffusion coefficient of the micelles,  $r$  the radius of drug particle, and  $D_{mol}$  the

molecular diffusion coefficient. The Damkohler number for the buffer phase ( $D_a$ ) is defined as follows:

$$D_a = \frac{12\emptyset r^2}{(1 - \emptyset)d_m^2} \quad (6)$$

where  $\emptyset$  is the volume fraction of micelles.  $D_a$  relates the rate at which micelles load with drug to the rate at which the drug diffuses through the buffer. The  $D_{am}$  value needed to fully equilibrate micelles depends on the drug particle size and the micelle size, because these will impact the diffusion time within the particle diffusion layer. This is captured by plotting  $D_{am}$  versus  $D_a$  and delineating the regions in which micelles should be equilibrated, empty, or in an intermediate zone. Such a plot is shown in Figure 3 (adapted from Sailaja et al.<sup>5</sup>) and it is referred to as a “phase space” plot for loading of micelles, following Kumar and Gandhi’s convention. The region above the red curve corresponds to  $D_{am} \gg 1 + D_a/D_{am}$  (see Sailaja et al. for details; exact derivation/ration-

alization beyond scope here). In this region,  $K_{eq}$  values are low and there are sufficient diffusional encounters between micelles and dissolved drug molecules to achieve the equilibrium saturated solution loading of micelles prior to leaving the diffusion layer. The region below the blue, dashed line corresponds to  $D_{am} \ll 1 + D_a/D_{am}$ .  $K_{eq}$  values are high in this regime and it is expected that the micelles leave the diffusion layer empty. To define the exact positions of the red and blue lines shown, we reproduce that used by

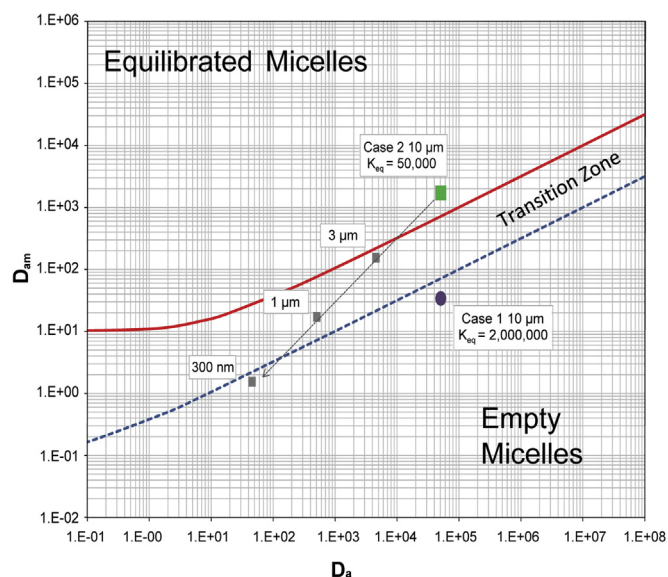


**Figure 3.** The relationship between  $D_{am}$  and  $D_a$  can provide prediction on loading of micelles when the values are plotted as shown (adapted from Sailaja et al.<sup>5</sup>). Equilibrated micelles are expected above the solid red line. Micelles typically exit the diffusion layer empty below the dashed blue line. A transition zone of “fractional loading” exists between the lines. Two model cases are included as described in the text. Case 1 parameters: 50  $\mu\text{g/mL}$  total solubility in SLS, 10 ng/mL solubility in pH 6.5 buffer, 10  $\mu\text{m}$  particle size distribution, and  $6 \times 10^{-6} \text{ cm}^2/\text{s}$  molecular diffusion coefficient. Case 2 differed only by increasing the buffer solubility to 0.5  $\mu\text{g/mL}$ , giving a concomitant approximately 50-fold decrease in  $K_{eq}$ .



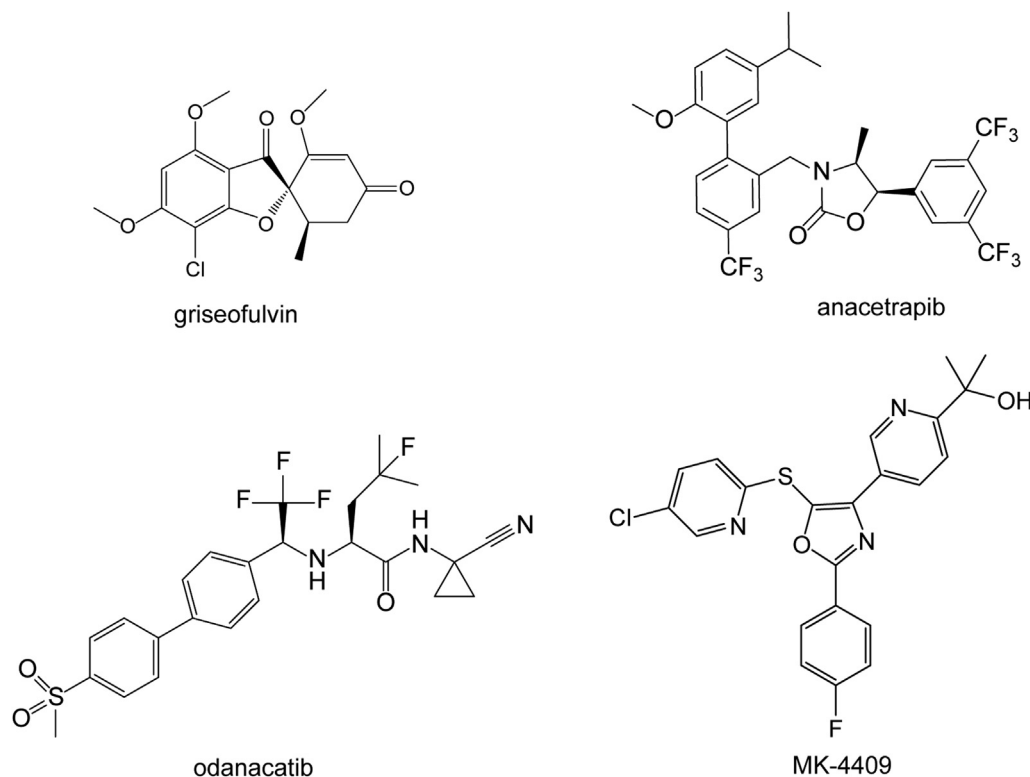


**Figure 4.** Structures of griseofulvin, anacetrapib, odanacatib, and MK-4409. Griseofulvin and anacetrapib have no  $pK_a$ . Odanacatib has  $pK_a$ s of 2.3 and 12.5 and MK-4409 has a  $pK_a$  of 3.5.

#### Micelle Diffusion Coefficient From Dynamic Light Scattering

Dynamic light scattering was performed on the dissolution media utilizing a Malvern Zetasizer (Malvern Instruments, Worcestershire, UK). Ten individual 10 s measurements were taken and averaged to indicate a single measurement of any sample of fluid. Samples were analyzed in triplicate and the data were averaged for any given aggregate particle size distribution result. Data were collected at room temperature and 37°C. Data were reported on a percent volume basis to ensure that higher signal intensity values for larger particles did not dominate the reported results. The micellar diffusion coefficient ( $D_{micelle}$ ) was determined from the Stokes-Einstein relation as follows:  $D_{micelle} = kT/6\pi\eta r$ , where  $k$  is the Boltzmann constant,  $T$  the absolute temperature,  $\eta$  the viscosity, and  $r$  the radius of the particle. The radius of the particle was assumed to be half the volume weighted average.

#### HPLC Analysis

Anacetrapib, odanacatib, and griseofulvin were analyzed by an Agilent 1100 HPLC with UV detection at 220 nm. MK-4409 was

analyzed with UV detection at 240 nm. Samples were injected neat (15  $\mu$ L) onto a 5 cm Waters Symmetry C18 column (3.5  $\mu$ m silica) at 35°C. The flow rate was 2 mL/min and the total run time was set to 7 min. The mobile phase consisted of a binary gradient of Solvent A (HPLC grade water with 0.1%  $H_3PO_4$ ) and Solvent B (acetonitrile). All 4 compounds were eluted under the following gradient: 60% A at initial, decreasing to 10% A in 5.0 min, followed by 10% A for 1.5 min, finally returning to starting conditions within 0.1 min. Quantitation of all compounds was made against gravimetrically prepared standards done in duplicate.

#### API Solubility and Molecular Diffusion Coefficient

Equilibrium solubilities in pH 6.5 blank buffer, 0.3% SLS, and FaSSIF were determined after 24 h saturation at 37°C. Insoluble materials were removed by centrifugation at 14,000 rpm for 5 min (Spectrafuge 16 M; Labnet Intl, Inc., Edison, NJ). Samples were injected neat onto the HPLC for determination of concentration.

The diffusion coefficients of the drug molecules ( $D_{mol}$ ) were determined from the molecular weights (MWs), as shown in Table 4. Equation 8 was used to calculate  $D_{mol}$  at 37°C.<sup>16</sup> The drug molecules discussed in this work have MWs ranging from 400 to 800 Da, and corresponding  $D_{mol}$  ranging from 4 to 7  $\times 10^{-6}$  cm<sup>2</sup>/s.

$$D_{mol}(\text{cm}^2/\text{sec}) = 10^{-4.113-0.4609 \times \log MW} \times 1.4 \quad (8)$$

#### Calculation of $K_{eq}$

$K_{eq}$  was calculated based on the following assumptions about the micelle volumes. For 0.3% SLS, the mass in 1 L, based on the MW and concentration, and the density in micelles (assumed to be

**Table 1**  
Composition of SLS and Biorelevant Media

Ingredient	0.3% SLS	FaSSIF
pH	6.5	6.5
NaH <sub>2</sub> PO <sub>4</sub>	28.4 mM	28.4 mM
NaOH	8.7 mM	8.7 mM
NaCl	105.6 mM	105.6 mM
SLS	10 mM	
NaTC		3 mM
Lecithin		0.75 mM

1.01 g/mL) were used to determine the volume of all SLS micelles. The concentration of molecules below the critical micelle concentration (CMC) was not included in the calculation of  $K_{eq}$ . We assumed that the CMC of SLS in 29 mM buffered media was 2.7 mM<sup>31</sup> and therefore the concentration of SLS molecules in micelles is 7.3 mM for 10 mM, 0.3% SLS. The calculation for FaSSIF was simplified by assuming that the micelle is entirely composed of lecithin, because NaTC has been shown to contribute to the mixed micelle system in a limited way.<sup>32</sup> For FaSSIF, the density was assumed to be 1.06 g/mL.

#### Dissolution of Dispersed Drug Particles

##### Pre-Dispersion of API

It was critical to ensure that the API was wetted and well-dispersed rapidly in the dissolution media. The APIs were suspended as a well-mixed slurry in buffered 0.3% SLS at 0.9–10 mg/mL, dependent on the final desired concentration in the vessel. The concentration in the dispersion was set so that no more than 3% of the API by weight was dissolved in the dispersion media prior to the start of the dissolution. The amount of API which was pre-dissolved was subtracted from the reported dissolution curves. The suspended API was stirred for 5 min at 300 rpm, sonicated for 5 min (Crest CP260 bath sonicator, power setting 8; Crest, Ewing, NJ), and then stirred for 5 min at 300 rpm. The dissolution test was started with the addition of the drug suspension to the media; total transfer times were typically <1 min for 6 vessels. The entire volume of media (1–15 mL) was added. The scintillation vials were thoroughly rinsed with media to remove as much of the API slurry as possible.

##### Target Drug Concentration

Given the drug particle dissolution rate information sought here, it was necessary to limit the amount of drug particle solids added to the micellar solutions to prevent the rapid saturation of the media with the poorly soluble drugs. Although working below approximately 10% solution saturation is ideal<sup>11,19,20</sup> in this regard, this can present HPLC quantitation challenges for the poorly soluble drugs in the fairly weak surfactant systems studied here. Drug solids were added equivalent to just saturating the micellar solution (this is termed 1× dissolution). This typically resulted in 10%–80% of the added solids dissolving over the 2 h dissolution period. In this concentration regime, the dissolution is sensitive to particle size<sup>11,19,20</sup> and micellar loading efficiency. The overall profiles are impacted by the decreasing solubility gap driving the dissolution, but this is readily accounted for in the DDDPlus™ dissolution modeling program.

##### Dissolution Apparatus and Method

Dissolution tests were performed with a VK7000 dissolution system with a VK7500 heater/circulator (Vankel Technologies, Inc., Cary, NC). The dissolution tests were carried out for 120 min in 900 mL of each dissolution media at 37°C with a USP II paddle speed of 100 rpm. Samples were drawn via glass pipettes at determined times and centrifuged at 14,000 rpm for 5 min. The dissolutions for 0.3% SLS and FaSSIF were performed in triplicate.

##### Nanoparticle Dissolution

Anacetrapib nanoparticles were created from amorphous solid dispersions consisting of 20% anacetrapib, 76.5%–78% copovidone, and 2%–3.5% TPGS (*D*- $\alpha$ -tocopheryl polyethylene glycol 1000 succinate, a surfactant). This HME amorphous solid dispersion forms 110 nm ( $D_{50}$ ) nanoparticles at 3.5% TPGS and 190 nm nanoparticles at 2% TPGS in water; the details of this mechanism are described

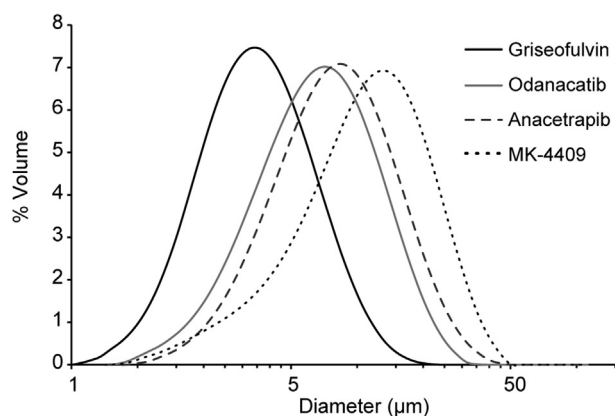


**Figure 5.** SLS measurements of the API size distribution. The  $D_{4,3}$  values are as follows: griseofulvin = 4.2  $\mu\text{m}$ , odanacatib = 6  $\mu\text{m}$ , anacetrapib = 7  $\mu\text{m}$ , and MK-4409 = 11  $\mu\text{m}$ .

elsewhere.<sup>30</sup> Approximately 20 mg of milled HME was weighed into a scintillation vial with 10 mL of stirring HPLC grade water at 37°C (300 rpm) for 1 h. An aliquot of the solution was spiked into 250 mL of FaSSIF as well as 250 mL of 0.3% SLS stirring at 300 rpm so that the total concentration was 0.6  $\mu\text{g/mL}$ . Ultracentrifugation (Optima TLX ultracentrifuge, TLA 110 rotor, 10 min at 348,000  $\times g$  (rmax)) was used to remove nanoparticles to measure molecularly dissolved anacetrapib. The experiment was carried out at 37°C through 2 h.

##### Simulation

A commercial dissolution modeling software, DDDPlus™ (version 5.0.0011; Simulations Plus, Inc., Lancaster, CA), was utilized for generating the *in silico* dissolution profiles for the APIs. The software has 3 main tabs: formulation, experimental setup, and simulation. In the formulation tab, a drug's physicochemical parameters are defined, including equilibrium solubility, diffusion coefficient, and targeted drug concentration. The  $D_{eff}$  value was calculated as described in the Theory section and entered as the diffusion coefficient. In the experimental setup tab, the apparatus type, instrument speed, medium volume, and medium type were specified. The particle size distribution of the API (Fig. 5) was used as an input parameter in DDDPlus™ to perform the simulations. Discreet bins were used in the distribution; no fitting was applied. A 2 h dissolution curve was simulated for each system.

##### Results

Figure 5 shows representative API size distributions measured by static light scattering (Malvern Mastersizer) as described in Methods. The  $D_{4,3}$  values of the compounds studied here range from about 4 to 20 microns and have fairly symmetric distributions.

##### Equilibrium Solubilities

The equilibrium solubilities of the APIs were measured in the following media, as prepared in the Methods section: pH 6.5 buffer, 0.3% SLS, and FaSSIF (Table 2). Griseofulvin's solubility matched well with that reported by Okazaki et al.<sup>13</sup> There is a significant range of reported buffer solubility values of itraconazole. Crisp et al.<sup>8</sup> uses a value of 1 ng/mL as reported by Peeters et al.,<sup>33</sup> but others have measured values over 1000 ng/mL.<sup>34</sup> Likewise, the reported values of danazol vary significantly. We determined the solubilities of danazol and itraconazole directly in Crisp et al.'s<sup>8</sup> pH 7.0 buffer preparation; their data were then interpreted in the context of our reported value.

**Table 2**  
Equilibrium Solubilities in Buffer and Micellar Media for Investigational Compounds

Solubilities	pH 6.5 Buffer ( $\mu\text{g/mL}$ )	0.3% SLS ( $\mu\text{g/mL}$ )	FaSSIF ( $\mu\text{g/mL}$ )
Odanacatib	0.39	30.0	1.0
Anacetrapib	0.040	22.1	6.0
Griseofulvin	9.7	233.0	12.0
MK-4409	0.010	14.4	1.0
Itraconazole <sup>8</sup>	0.040 <sup>a</sup>	10.0	
Danazol <sup>8</sup>	0.88 <sup>a</sup>	67.0	
Danazol <sup>13</sup>	0.21		18.0
Griseofulvin <sup>13</sup>	10.4		15.4

Values for danazol, griseofulvin, and itraconazole in micellar media are taken from the literature where noted; danazol and itraconazole in pH 7.0 buffer were measured in-house.

<sup>a</sup> pH 7.0 buffer, as prepared by Crisp et al.<sup>8</sup>

### Diffusivities

The values of  $D_{\text{micelle}}$  depend on the aggregate size. Although the size of SLS micelles has been well described,<sup>35,36</sup> more variability in FaSSIF aggregate sizes has been reported.<sup>37,38</sup>  $D_{\text{micelle}}$  was determined based on the aggregate size in our homemade media preparations and the Stokes-Einstein relation (Table 3). The diameters of the micelles were measured by dynamic light scattering as described in the Methods section. The diffusion coefficients of the drug molecules were calculated by Equation 8 and are listed in Table 4.

The solubilities,  $D_{\text{mol}}$ , and  $D_{\text{micelle}}$  were used to determine  $D_{\text{eff}}$  according to Equation 2. For each molecule, a lower bound is set where the micelles cannot contribute to the mass transfer. The second term in the  $D_{\text{eff}}$  equation goes to zero in this case; this is referred to as  $D_{(0\% \text{ loaded})}$ . The mass transfer is described by Equation 3. Table 5 lists the  $p$  value for each molecule, the determination of which will be described in detail in the Discussion section. The first and second terms of Equation 7 are also given for each molecule in Table 5, as well as the ratio between them. Additionally, Table 5 compares  $D_{\text{eff}}$  corresponding to  $p = 1$  with that which was observed in each system ( $D_{\text{observed}}$ ).

### $K_{\text{eq}}$

$K_{\text{eq}}$  was calculated as described in the Methods sections and Equation 4.

### Dissolution of Dispersed Drug Particles in 0.3% SLS

Figures 6a-6d show the dissolution data obtained in this work (red squares) for the dispersed drug particle populations of griseofulvin, odanacatib, MK-4409, and anacetrapib in 0.3% SLS. The solid green curves show the DDDPlus<sup>TM</sup> calculated dissolution profiles expected using the Nernst-Brunner assumptions with fully equilibrated micelles (Eq. 3 or 7 with  $p = 1$ ). Also shown in each panel is the predicted contribution of drug mass transport into solution due to the buffer phase alone (blue curves) as described in the Theory section (Eq. 7 with  $p = 0$ ). For each drug, the calculated green and blue curves will reflect the relative sizes of  $D_{\text{eff}}$  and

**Table 3**  
Calculation of Diffusion Coefficients From Stokes-Einstein Relation and Measured Aggregate Diameter

Aggregate System	$D_{50}$ (nm)	Diffusion Coefficient ( $\times 10^{-6} \text{ cm}^2/\text{s}$ )
0.3% SLS	3.7	1.8
FaSSIF	13	0.50

$D_{(0\% \text{ loaded})}$  shown in Table 5. The  $K_{\text{eq}}$  values from Table 6 are also provided on each plot. The dissolution data in panels a and b show remarkably good agreement with the Nernst-Brunner fully equilibrated micelle (green) curves. This indicates that efforts to disperse the particles in the dissolution media to the same degree measured using the Malvern particle sizing instrument have been successful. Panels c and d show dissolution data which are much slower than the fully equilibrated micelle calculation. MK-4409 data appear generally described by use of  $p = 0.10$  in Equation 7, while anacetrapib data appear consistent with  $p = 0$  in Equation 7.

### Dissolution of Dispersed Drug Particles in FaSSIF

Figures 7a-7d show the dissolution data obtained in this work (red squares) for the dispersed drug particle populations of griseofulvin, odanacatib, MK-4409, and anacetrapib in FaSSIF. Figure 7 shows the solid green and blue curves for  $D_{\text{eff}}$  and  $D_{(0\% \text{ loaded})}$  and are described in Figure 6. The  $K_{\text{eq}}$  values from Table 6 are also provided on each plot. The dissolution data in panels a and b seem well described by the Nernst-Brunner fully equilibrated micelle (green) curves. Note that the green and blue curves are similar, as would be expected due to the similarity of  $D_{\text{eff}}$  and  $D_{(0\% \text{ loaded})}$  for these molecules in FaSSIF (Table 5). Panels c and d show dissolution data which are much slower than the fully equilibrated micelle calculation. MK-4409 data appear generally described by use of  $p = 0.80-0.85$  in Equation 7, while anacetrapib data appear consistent with  $p = 0.01$  in Equation 7.

### Discussion

#### Micelle Loading in SLS: Can the Indirect Micelle Loading Mechanism Provide a Plausible Rationale for "Slow" Dissolution Rates?

Figure 6 shows that MK-4409 and anacetrapib exhibit dissolution much slower than predicted by Nernst-Brunner assumptions with equilibrium loaded micelles. We are not the first to note such slow dissolution from dispersed drug particles in SLS solutions. Williams and Johnston<sup>8</sup> similarly reported this effect for itraconazole and danazol in 0.3% SLS solutions. They interpreted their data only in the context of the Cussler mechanism in Figure 1a, such that micelles must be fully loaded upon their desorption into the particle diffusion layer. To account for the diminished mass transfer, they postulated that there must be much slower rate-limiting steps in the formation of the drug loaded micelle at the particle surface (Fig. 1a, steps 2-4). These unknown surface processes were grouped into an interfacial reaction rate constant,  $k_s$ . The slow dissolution data for the largest 2.4  $\mu\text{m}$  ( $D_{50}$ ) itraconazole particles and 1.6  $\mu\text{m}$  ( $D_{50}$ ) danazol particles were rationalized by  $k_s$  values which were approximately 40 and 10 times smaller, respectively, than the Nernst-Brunner mass transfer rate predictions with equilibrated micelles.

The indirect loading mechanism described by Kumar and Gandhi would predict that slow dissolution is possible if the drug particle/surfactant system lies in the transition or empty micelle region of the appropriate phase space plot (Fig. 3). The Damkohler numbers  $D_{\text{am}}$  (Eq. 5) and  $D_a$  (Eq. 6) are calculated for the compounds studied here, as well as for 2.4 and 1.6  $\mu\text{m}$  itraconazole and danazol reported by Crisp et al.<sup>8</sup> The resulting phase space plot of  $D_{\text{am}}$  versus  $D_a$  is shown in Figure 8. Nearby each data point (each representing a drug compound  $D_a$ ,  $D_{\text{am}}$  pair) on the phase plot is included the % micellar loading found from estimating values of  $p$  in Equation 7 as described above. For itraconazole and danazol, the 2.4  $\mu\text{m}$  and 1.6  $\mu\text{m}$  particle distributions and amount of drug solids per milliliter were imported from Crisp et al.'s<sup>8</sup> manuscript and then their dissolution profiles fit with Equation 7, varying  $p$ , to estimate

**Table 4**  
Log *P*, Molecular Weight, and Molecular Diffusion Coefficients as Determined by Equation 8

Drug Molecule	Log <i>P</i>	Molecular Weight	Diffusion Coefficient ( $\times 10^{-6}$ cm <sup>2</sup> /s)
Anacetrapib	8.8	637.52	5.13
Odanacatib	2.9	527.57	5.68
Griseofulvin	2.2 <sup>34</sup>	352.76	7.05
MK-4409	3.6	441.00	6.25
Danazol	0.50 <sup>35</sup>	337.50	7.21
Itraconazole	5.7	705.64	4.86

the % loading identically to the treatment of the data presented here.

The overall view of the solid data points in Figure 8 with the % loading values found here appears remarkably consistent with the indirect loading mechanism. All 4 cases where dissolution was slower than Nernst-Brunner assumptions (with equilibrated micelles) fall cleanly into the region where indirect loading processes are predicted to be unable to equilibrate micelles within particle diffusion layers. In this view, itraconazole and danazol show only 3% and 9%, respectively, of their equilibrated mass fractions of the drugs in the micelle phase by the time the SLS micelles leave the particle diffusion layers, while MK-4409 and anacetrapib achieve approximately 10% and 0% (essentially empty) micelle loading. Thus in the indirect micelle loading framework, this slow dissolution is still due to a diffusion controlled process—the diffusion of incompletely loaded micelles out of the particle diffusion layer. We should emphasize that the dissolution profile data itself cannot distinguish between either models. Our values of *p* derived here are closely related to the ratio of Williams and Johnstons and coworkers<sup>18</sup> *k<sub>s</sub>* rate divided by the fully equilibrated (Nernst-Brunner) predicted dissolution rate (i.e., the dissolution profiles shown here can be fit similarly either way). The open data points in the Figure 8 phase plot are described below.

#### Micelle Loading in FaSSiF: Direct or Indirect Loading?

Figure 7 shows that MK-4409 and anacetrapib exhibit dissolution profiles in FaSSiF which are much slower than predicted by Nernst-Brunner assumptions with equilibrium loaded micelles. Sugano and coworkers<sup>13</sup> reported dispersed particle dissolution data in FaSSiF for griseofulvin ( $D_{50} = 7 \mu\text{m}$ ) and danazol ( $D_{50} = 22 \mu\text{m}$ ). Micelles were assumed to be fully loaded to their saturated equilibrium values within particle diffusion layers. Although griseofulvin gave the expected dissolution rate, danazol showed 20%–30% slower dissolution rates than predicted. The FaSSiF data in

**Table 5**  
Calculated Terms of Equation 7 and the Ratio Between Them,  $D_{\text{eff}}$ , and  $D_{(\text{observed})}$  for Drug Molecules in Two Micellar Systems

0.3% SLS	$D_{(0\% \text{ loaded})}$ ( $D_{\text{mol/mol}}$ ) ( $\times 10^{-6}$ cm <sup>2</sup> /s)	<i>p</i>	$D_{(\text{micelle phase})}$ ( $pD_{\text{micelle/micelle}}$ ) ( $\times 10^{-6}$ cm <sup>2</sup> /s)	Ratio of $D_{(\text{micellar})}$ to $D_{(0\% \text{ loaded})}$	$D_{\text{eff}}$ ( $\times 10^{-6}$ cm <sup>2</sup> /s)	$D_{(\text{observed})}$ ( $\times 10^{-6}$ cm <sup>2</sup> /s)
0.3% SLS						
Odanacatib	0.073	1	1.8	24	1.8	1.8
Anacetrapib	0.0093	0	0	0	1.8	0.0093
Griseofulvin	0.29	1	1.7	6	2.0	2.0
MK-4409	0.0043	0.1	0.18	41	1.8	0.18
Itraconazole (Williams <sup>8</sup> 2.4 $\mu\text{m}$ )	0.020	0.03	0.054	3	1.8	0.073
Danazol (Williams <sup>8</sup> 1.6 $\mu\text{m}$ )	0.095	0.09	0.16	2	1.9	0.25
FaSSiF						
Odanacatib	2.2	1	0.31	0.1	2.5	2.5
Anacetrapib	0.034	0.01	0.0050	0.2	0.53	0.039
Griseofulvin	5.8	1	0.096	0.02	5.8	5.8
MK-4409	0.062	0.8	0.40	6	0.56	0.46
Griseofulvin (Sugano <sup>13</sup> )	4.8	1	0.16	0.03	4.9	4.9
Danazol (Sugano <sup>13</sup> )	0.084	0.8	0.40	5	0.58	0.48

Figure 7 and Sugano and coworkers<sup>13</sup> FaSSiF data are examined within the context of the indirect loading mechanism and Kumar and Gandhi's micellar loading phase space plots as shown in Figure 8 for SLS. The Damkohler numbers  $D_{\text{am}}$  (Eq. 5) and  $D_a$  (Eq. 6) and the phase space plot of  $D_{\text{am}}$  versus  $D_a$  are determined as described above and the result is shown in Figure 9 along with the % loading estimates from Equation 7. The phase space positioning of griseofulvin measured in-house aligns well with Sugano and coworkers<sup>13</sup>—the offset being due primarily to differences in size.

The overall behavior of the set of drugs in Figure 9 with the associated % loading values again is consistent with the indirect loading mechanism. All cases where dissolution was slower than Nernst-Brunner assumptions (with equilibrated micelles) approach the region where indirect loading processes are predicted to be unable to equilibrate micelles within particle diffusion layers. Griseofulvin is 100% loaded in the diffusion layer and is well-described by Equation 3. The data for danazol and MK-4409, on the other hand, achieve only 80% of their theoretical dissolution rates. Anacetrapib is limited to 1% micelle loading. In this context, diffusion of micelles and solubilized drug in buffer would again be the rate-limiting steps of the particle dissolution process.

A more detailed consideration of the actual micellar compositions present in FaSSiF, in our view, suggests that direct loading in FaSSiF is difficult to rationalize. It has long been known that biologically relevant lecithins do not associate into micelles when added to water<sup>39,40</sup>; it is the NaTC in the FaSSiF that serves to solubilize the lecithin monomers. However, Carey et al.<sup>32,40</sup> describe the NaTC phase diagram for the NaTC-lecithin system and find that only approximately 10% or less of the NaTC present in FaSSiF participates in the stabilization of the lecithin-NaTC aggregates. In the 3 mM NaTC, 0.75 mM lecithin concentration regime, the lecithin-NaTC aggregates may be vesicular to disk-like in shape and are considered to be in a metastable phase. The remaining <3 mM NaTC is generally considered below the poorly defined CMC range of 3–12 mM<sup>41</sup> and does not contribute to the solubility in FaSSiF of any of the compounds in Table 2 at 3 mM (solubilities measured at 3 mM NaTC, data not shown). It can be expected that some portion of the negatively charged NaTC present partitions onto drug particle surfaces. In this context, it is difficult to rationalize how FaSSiF micelles could directly solubilize solute at the drug particle surface. Cussler's mechanism (Fig. 1a) would imply that as the micelle approaches the surface, detergent molecules diffuse through the bulk solution to the surface. Lecithin is practically insoluble in water; there would be low driving force for monomers to leave the mixed micelles in order to diffuse to a surface to form the lecithin-rich micelle which is actually solubilizing dissolved drug molecules in the FaSSiF system.

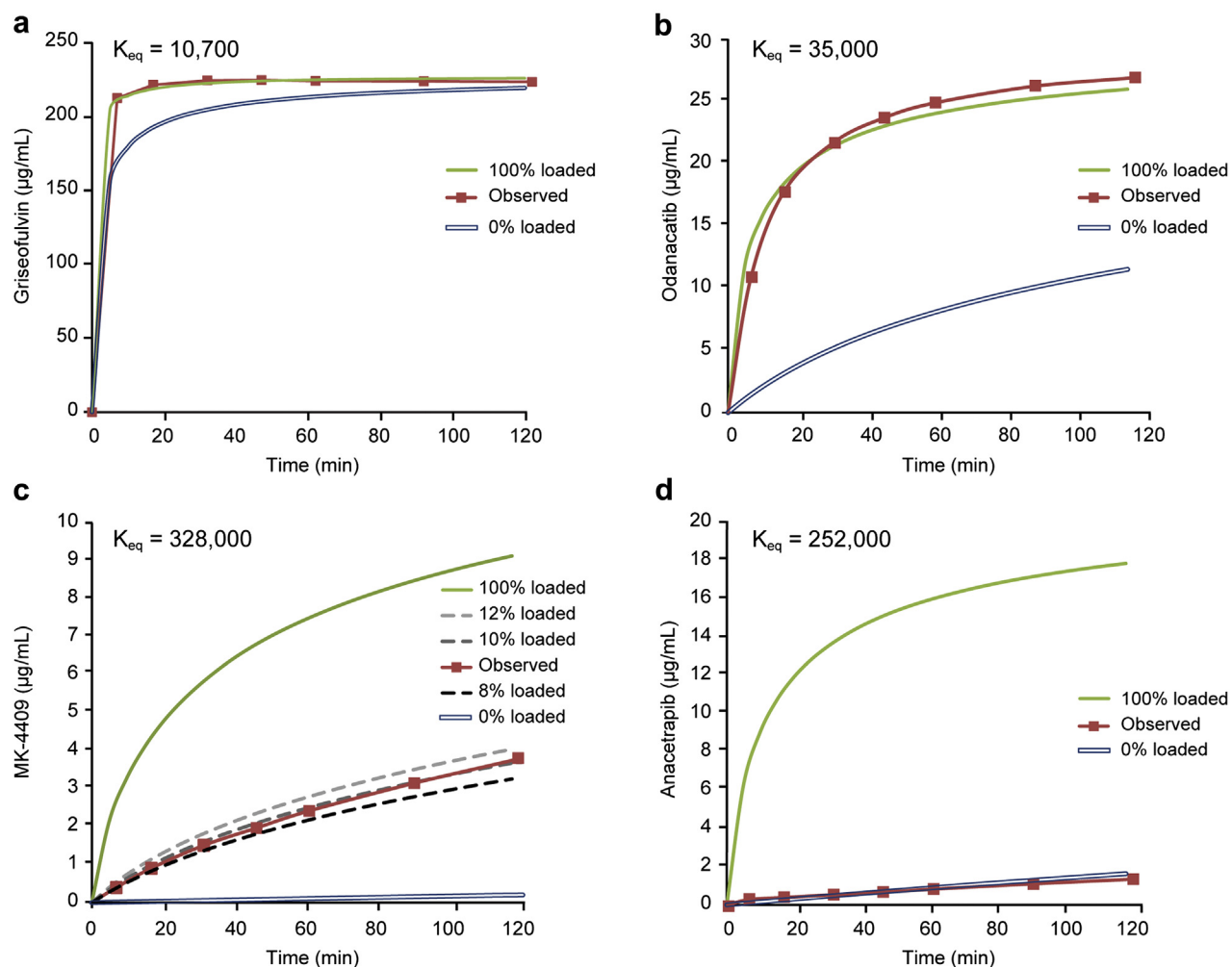


**Figure 6.** Observed versus modeled dissolution data for (a) griseofulvin, (b) odanacatib, (c) MK-4409, and (d) anacetrapib in 0.3% SLS.

#### Pharmaceutical Implications: Indirect Versus Direct Micelle Loading Processes in Ionic Surfactant Systems SLS and FaSSiF

If drug particle dissolution rates were always well predicted by Nernst-Brunner assumptions, then attempting to rationalize the indirect or direct loading mechanism would be a largely theoretical exercise. However, the existence of drug particle distributions with significantly slower dissolution offers an opportunity to compare the loading mechanisms. For example, the occurrence of slower dissolution rates is easily predicted in the indirect micelle loading framework. In the indirect micelle loading framework, slow particle dissolution rates occur when the  $K_{eq}$  values are large enough to drive the ( $D_a$ ,  $D_{am}$ )

**Table 6**  
 $K_{eq}$  in Two Media

$K_{eq}$	0.3% SLS	FaSSiF
Odanacatib	35,000	3000
Anacetrapib	252,000	278,000
Griseofulvin	11,000	400
MK-4409	328,000	122,000
Griseofulvin <sup>8</sup>		900
Danazol (7 µm) <sup>8</sup>		158,000
Danazol (1.6 µm) <sup>13</sup>	35,000	
Itraconazole <sup>13</sup> (2.4 µm)	114,000	

The 4 investigational compounds (odanacatib, anacetrapib, griseofulvin, and MK-4409) are compared to literature values of griseofulvin, itraconazole, and 2 size distributions of danazol.

data point into the transition or empty region of the micelle loading phase space plot. In this context, it is worthwhile to note that 2 drugs with similar, low solubility values in SLS or FaSSiF (e.g., 50 µg/mL) can give either the Nernst-Brunner expected dissolution rate or much slower, depending on buffer solubility value (see example in Fig. 3). Determination of  $K_{eq}$  requires only an equilibrium solubility measurement in buffer and in SLS or FaSSiF. In contrast, Williams and Johnston and coworkers<sup>8</sup> and more recently Shekunov<sup>29</sup> noted in the direct micelle loading framework that slow dissolution controlled by micellar surface formation/desorption kinetics ( $k_s$  or  $\beta_0$ , respectively) is not readily predicted or understood from a consideration of the material properties of the surfactant and the drug.

Another important area to compare both mechanisms is in terms of what degree of dissolution rate improvements can be expected upon particle size reduction (e.g., from approximately 5 to 20 micron drug particles down to the several hundred nanometer range). This topic has been of increased interest given the prevalence of poorly soluble drugs in today's pharmaceutical pipelines.<sup>8,29,42-48</sup> In the direct loading model, if particle dissolution is controlled by  $k_s$  or  $\beta_0$  then the dissolution rate will scale with the surface area of the particle ensemble. At fixed mass, the ensemble surface area increases as  $1/r$ . Any reduction in the particle diffusion layer thickness (as particle size is reduced) has no impact in this model, as diffusion is not the rate-limiting step.<sup>8,29</sup> Crisp et al.<sup>8</sup> studied a range of 2.4 µm to 240 nm ( $D_{50}$ ) itraconazole particles and 1.6 µm to 300 nm ( $D_{50}$ ) danazol drug particles in SLS and NaTC

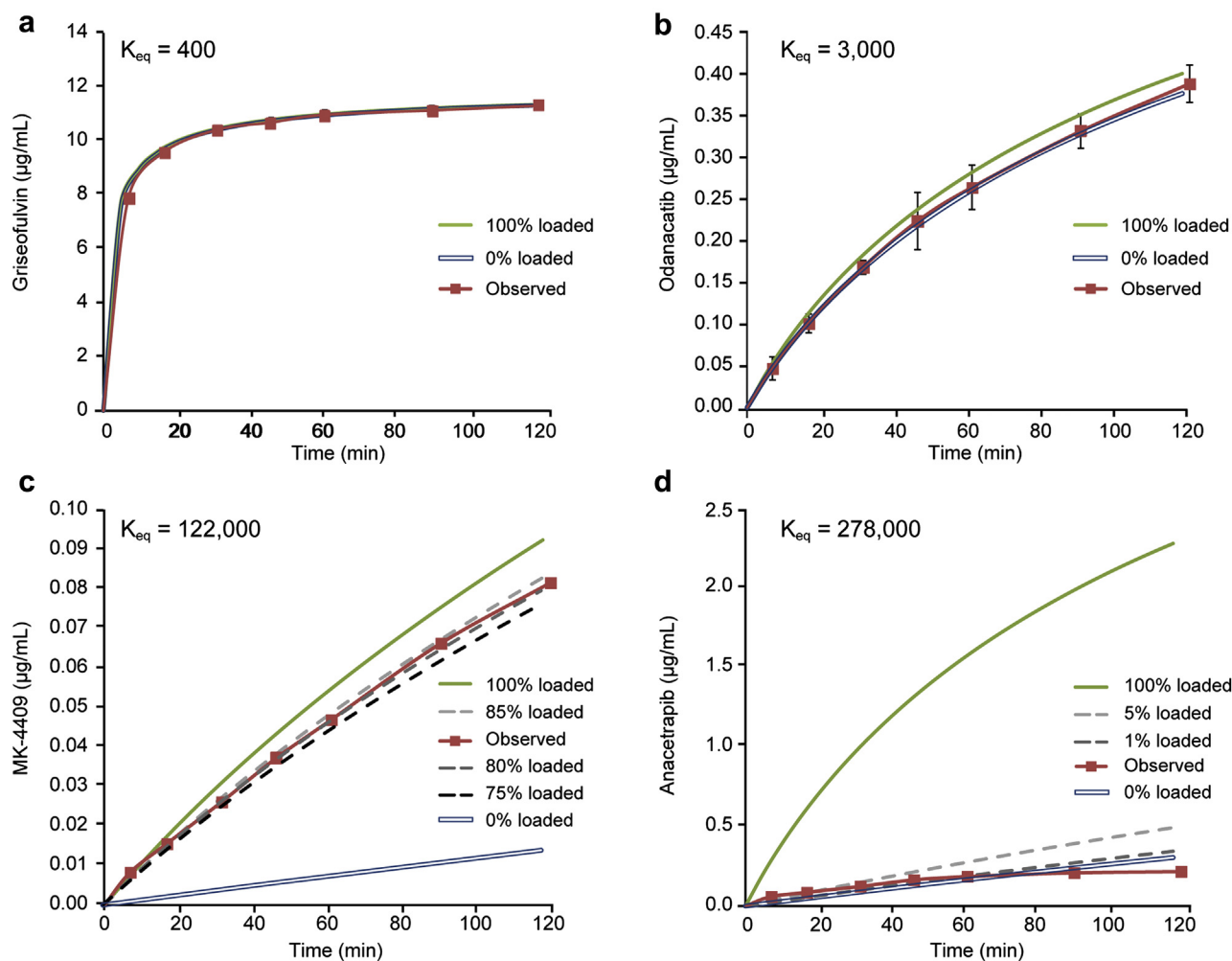


**Figure 7.** Observed versus modeled dissolution data for (a) griseofulvin, (b) odanacatib, (c) MK-4409, and (d) anacetrapib in FaSSiF.

and found that initial dissolution rates increased only 10%–20% faster than  $1/r$  (or as  $\sim 1/r$  in the case of itraconazole in SLS). These findings appear generally consistent with the direct loading,  $k_s$  or  $\beta_0$  controlled particle dissolution model for these 2 drugs.<sup>8,29</sup>

We develop here for comparison the dissolution rate enhancement predicted by the indirect loading mechanism upon particle size reduction. Initially, the process is diffusion-controlled as described above and the diffusion layer thickness changes with the particle radius. It is generally accepted<sup>9,49–51</sup> that in Equation 1  $\delta$  scales with the particle radius or diameter below a particle size of about 30 microns. Galli<sup>52</sup> has verified this relationship down to  $r$  values of  $\sim 500$  nm for a drug molecule in water, and we assume it to operate for all  $r$  values examined here. Overall, this gives in Equation 1 a dissolution rate which should increase as  $1/r^2$  as the particle size is reduced. For convenience, if the dissolution time of a particle is considered (proportional to  $1/\text{dissolution rate}$ ) this leads to the well-known equation<sup>53</sup> for predicting a particle's dissolution time at infinite dilution in the case of water or buffer:

$$T_{\text{infin}} = \frac{r_0^2 \rho}{3C_S D_{\text{mol}}} \quad (9)$$

where  $r_0$  is the initial radius in cm,  $\rho$  the density in  $\text{g/cm}^3$ ,  $D_{\text{mol}}$  the molecular diffusion coefficient, and  $C_S$  the solubility limit of the drug in buffer ( $\text{g/cm}^3$ ).

Equation 9 can now be modified for the contribution of micelles, by substituting  $D_{\text{eff}}$  from Equation 2 in the same way that led to Equation 7. The modified form of Equation 9 describing the time for the drug particle to dissolve given the indirect loading framework is

$$T_{\text{infin}} = \frac{r_0^2 \rho}{3C_T [D_{\text{mol}} f_{\text{mol}} + p D_{\text{micelle}} f_{\text{micelle}}]} \quad (10)$$

where all parameters are as defined in Equation 7. Note that when  $p = 0$  (no contribution by micelles),  $f_{\text{mol}} = C_S/C_T$  that the denominator in Equation 10 collapses to that in Equation 9 which describes the particle dissolution only in buffer. The key feature revealed in Equation 10 is to recognize that the value of  $p$  in the denominator is dependent on the particle radius. Decreasing the drug particle size means fewer and fewer diffusional encounters between micelles and dissolved drug molecules in the diffusion layer. This effect is shown in Figure 3 for the case 2 example, where for a 10 micron particle the  $p$  value should be 1.0, while at a 300 nm particle size, micelles are predicted to leave the diffusion layer empty ( $p = 0$ ). The 300 nm particle in this example will exhibit a dissolution rate due entirely from mass transport through the buffer phase alone (described by Eq. 9). Thus in the indirect micelle loading paradigm, poorly soluble drugs can have substantial decreases in their total diffusivity (term in brackets in Eq. 10) as  $p$  values drive toward zero as the particle size is reduced.

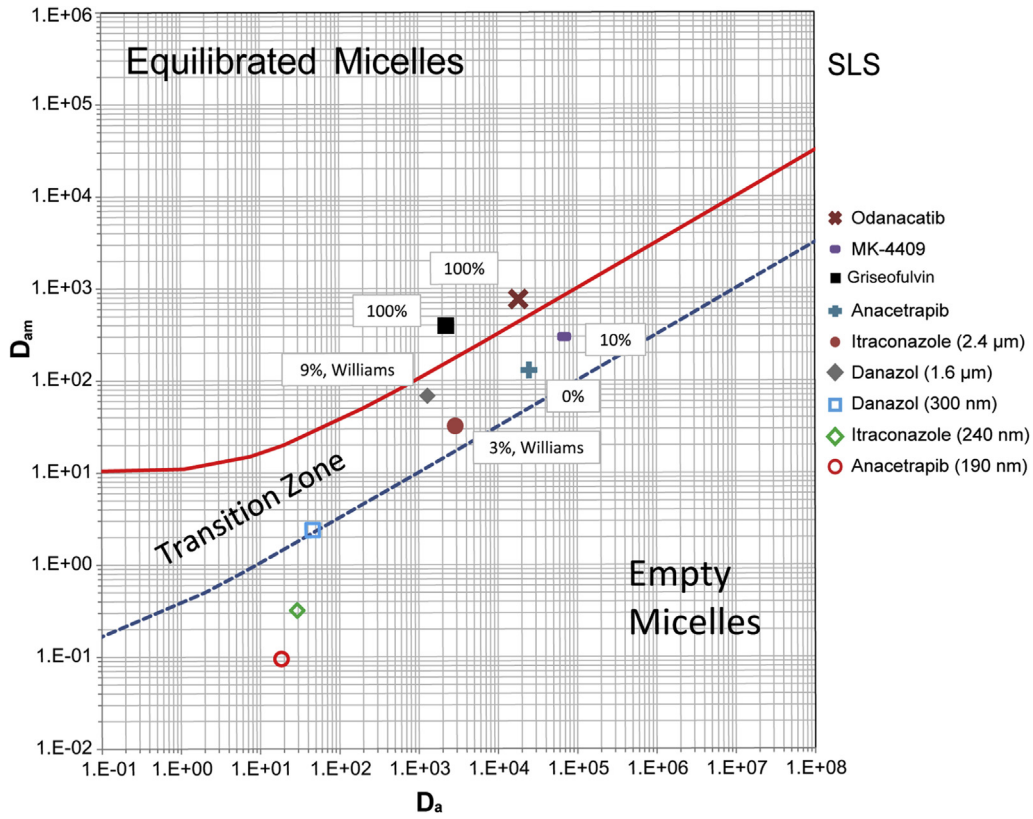


**Figure 8.** A total of 0.3% SLS phase space. Solid data points with percent loading values from Equation 7. Open data points highlight the location of 190-300 nm  $D_{50}$  populations of danazol, itraconazole, and anacetrapib.

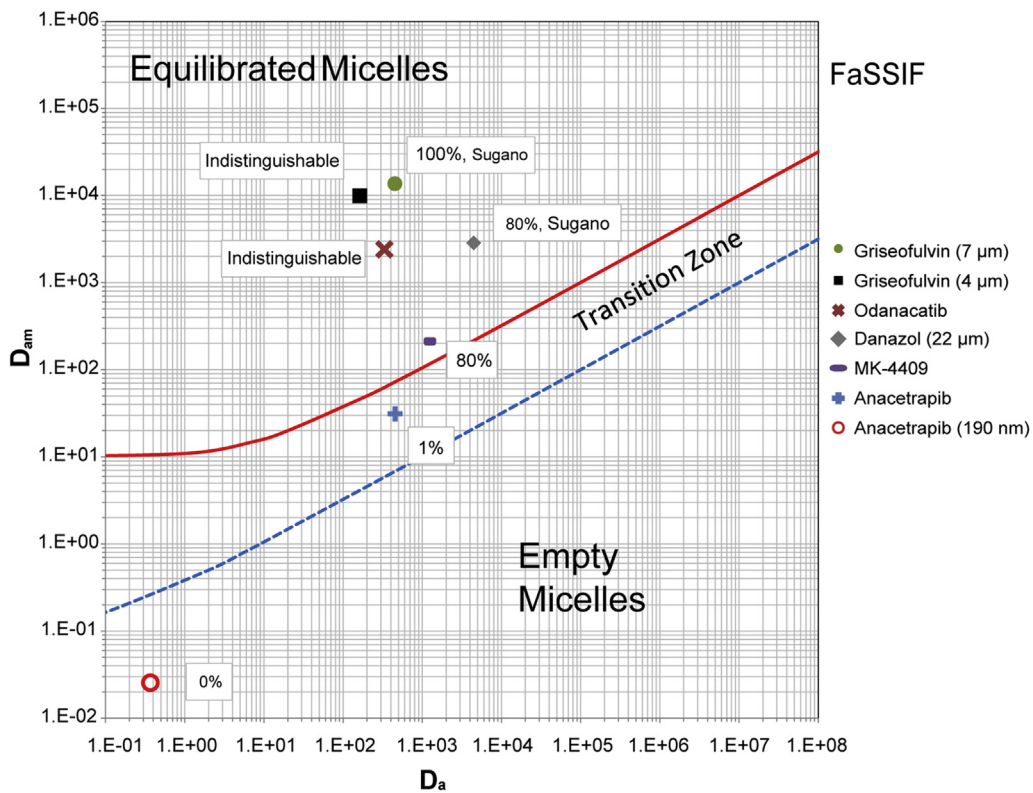


**Figure 9.** FaSSIF phase diagram. Solid data points with percent loading values from Equation 7. The open data point highlights the location of the 190 nm  $D_{50}$  populations of anacetrapib.

**Table 7**  
 $T_{\text{infin}}$  Dependence on Size for Danazol and Itraconazole

Variable	$T_{\text{infin}}$ (Observed)	$T_{\text{infin}}$ (Eq. 10)	Ratio If $r^2$ Is Assumed	Ratio If $r$ Is Assumed
Danzol (300 nm)	~10 s	15 s		
Danzol (1600 nm)	~90 s	165 s		
$T_{\text{infin}}$ ratio	~9	11	28	5
Itraconazole (240 nm)	~10 min	5.2 min		
Itraconazole (2400 nm)	~150 min	140 min		
$T_{\text{infin}}$ ratio	~15	25	100	10

For danazol (300 nm) and itraconazole (240 nm),  $p = 0$  in Equation 10; for danazol (1600 nm),  $p = 0.09$ ; and for itraconazole (2400 nm),  $p = 0.03$ .

It is worthwhile to apply Equation 10 to the largest and smallest danazol and itraconazole particles studied by Crisp et al.<sup>8</sup> in 0.3% SLS. The open data points in Figure 8 show the location of the 300 nm danazol and 240 nm itraconazole systems. It is assumed that  $p = 0$  for both these nanoparticles due to their locations on the phase space. Table 7 summarizes the observed  $T_{\text{infin}}$  values (simple linear extrapolation of the slope from the first approximately 0%-20% dissolved to 100% dissolved from Crisp et al.'s<sup>8</sup> dissolution data);  $T_{\text{infin}}$  values calculated by Equation 10, as well as the  $r^2$  and  $r$  changes across the particle range.

This treatment shows fairly good agreement between predicted  $T_{\text{infin}}$  values and those estimated from the dissolution data. Here the smallest nanoparticles'  $T_{\text{infin}}$  values derive from mass transport from buffer solubilization alone, danazol being much faster due to much higher buffer solubility (22-fold higher). In all cases, the agreement is within a factor of approximately 2 or better. Again, the indirect micelle loading mechanism appears to be a plausible construct to describe the observed poorly soluble drug particle dissolution rates. Note in Table 7 that decreasing the  $p$  value to zero across the 2  $\mu\text{m}$  to 300 nm region leads to a significant diminishment in the expected  $T_{\text{infin}}$  improvements compared to  $r^2$  dependence.

#### Anacetrapib Nanoparticle Dissolution Provides an Example of a Final Dissolution Rate-Limiting Step in the Indirect Micelle Loading Mechanism

In the indirect micelle loading mechanism as treated above, micelles load only through encounters with drug dissolved into the buffer phase. However, the dissolution of drug into the buffer phase is assumed to be fast (relative to diffusion out of the particle diffusion layer) in Equations 2, 3, 7, 9, and 10. As the drug particles are made smaller and smaller, this may not be the case. The actual solubilization rate of the drug into the buffer may begin to further impact the particle dissolution rate (this rate has been recently

referred to as the surface kinetic coefficient without micelles,  $\beta_{01}$ ).<sup>8,29</sup> Anacetrapib nanoparticle dissolution rates provide an illustrative example. A total of 110 and 190 nm ( $D_{50}$ ) anacetrapib nanoparticles are created from an anacetrapib HME formulation previously described.<sup>30</sup> Anacetrapib has approximately 4-fold higher solubility in 0.3% SLS media than in FaSSIF media, and the SLS micelles have nearly 4-fold higher diffusivity values due to their smaller size (Table 3). Figure 10 shows the dissolution data over the first 30%-50% of the 0.6  $\mu\text{g}/\text{mL}$  anacetrapib nanoparticles added to both micellar solutions. The dissolution rates of the anacetrapib nanoparticles are identical in these 2 very different surfactant systems. In the direct micelle loading context, one might expect different nanoparticle dissolution rates in these 2 different surfactant systems. However, in the case of indirect micelle loading, the  $p$  values are 0 in Equation 10 for these nanoparticles (open data points, Figs. 8 and 9) and thus the dissolution process should be mediated only through the buffer phase, thus predicting identical dissolution rates in either SLS or FaSSIF.

Application of Equation 10 to the 190 nm  $D_{50}$  population (e.g.) with  $p = 0$  predicts a  $T_{\text{infin}}$  of about 3.5 min. The % dissolved data in Figure 10 give an extrapolated  $T_{\text{infin}}$  value of closer to 80 min—a factor of 20-25 slower than expected due to the mass transfer rate from the buffer (danazol and itraconazole agreement in this same limit was within a factor of 2 above as noted above). We conclude this reflects that solubilization of drug into the buffer at the particle surface ( $\beta_{01}$  rate) has become rate-limiting. In our view, this is likely related to the unusually high lipophilicity of anacetrapib, having a log  $P$  of 8.8 (Table 4). We note in this context in Table 7 that the 240 nm itraconazole particles (log  $p = 5.7$ ) are 2-fold slower than predicted by Equation 10, and it is possible that the itraconazole  $\beta_{01}$  value is largely accountable for this difference. Thus in the indirect loading mechanism, as drug particle size is reduced to the several hundred nanometer region,  $\beta_{01}$  rates in combination with  $p$  values approaching zero in Equation 10 can lead to much weaker improvements in  $T_{\text{infin}}$  that can approach only an  $r$  dependence (Table 7) rather than the  $r^2$  dependence expected from a diffusion-controlled Nernst-Brunner dissolution process.

#### Conclusions

Kumar and Gandhi's indirect micelle loading mechanism (Fig. 1b) for ionic surfactants has been explored as a plausible alternative to Cussler's direct loading mechanism (Fig. 1a) which has been widely assumed in the pharmaceutical context. The dissolution profiles of the 4 drug molecules studied here and previous data reported by Sugano and coworkers<sup>13</sup> and Williams and Johnston and coworkers<sup>8</sup> are reasonably described by either mechanism. However, in the indirect micelle loading framework, slower dissolution rates (compared to Nernst-Brunner assumptions) can be predicted for drugs with increasingly larger  $K_{\text{eq}}$  values. On the other hand, slow particle dissolution in the direct micelle loading mechanistic framework is more difficult to predict from drug or surfactant properties. We develop a view of the dissolution

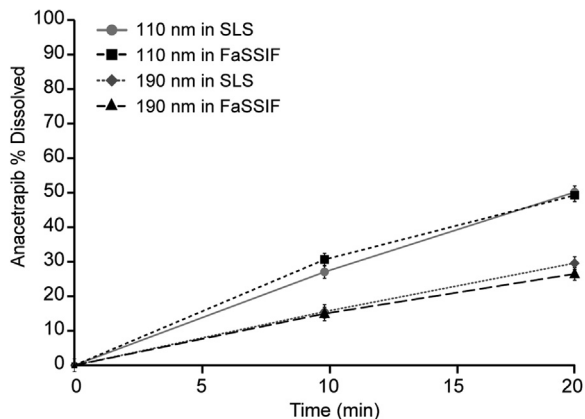


**Figure 10.** Dissolution of anacetrapib nanoparticles in FaSSIF and 0.3% SLS at 0.6  $\mu\text{g}/\text{mL}$ .

rate enhancements expected from drug particle size reduction assuming indirect micelle loading. Equation 10 and Figures 3, 8, and 9 highlight the primary result that as drug particles are made smaller,  $p$  will approach zero and drug nanoparticle mass transport out of the diffusion layer proceeds entirely through the buffer phase. This is a different view of nanoparticle dissolution than described in the direct micelle loading mechanistic framework. Anacetrapib nanoparticles (log  $P$  8.8) provides a clear example of a further limit operating in the indirect loading mechanism, in which the actual drug solubilization into the buffer alone (the kinetic coefficient  $\beta_{01}^{29}$ ) can become the rate-controlling step in drug nanoparticle dissolution.

## Acknowledgment

The authors would like to thank Merck & Company, Inc., Kenilworth, NJ, for all financial support.

## References

- Lipinski CA. Drug-like properties and the causes of poor solubility and poor permeability. *J Pharmacol Toxicol Methods*. 2000;44(1):235-249.
- Sugano K, Okazaki A, Sugimoto S, Tavorivipias S, Omura A, Mano T. Solubility and dissolution profile assessment in drug discovery. *Drug Metab Pharmacokinet*. 2007;22(4):225-254.
- Lennernaas H, Aarons L, Augustijns P, et al. Oral biopharmaceutics tools—time for a new initiative—an introduction to the IMI project OrBiTo. *Eur J Pharm Sci*. 2014;57:292-299.
- Chan AF, Fennell Evans D, Cussler EL. Explaining solubilization kinetics. *Am Inst Chem Eng J*. 1976;22(6):1006-1012.
- Sailaja D, Suhasini KL, Kumar S, Gandhi KS. Theory of rate of solubilization into surfactant solutions. *Langmuir*. 2003;19(9):4014-4026.
- Balakrishnan A, Rege BD, Amidon GL, Polli JE. Surfactant-mediated dissolution: contributions of solubility enhancement and relatively low micelle diffusivity. *J Pharm Sci*. 2004;93(8):2064-2075.
- Crison JR, Shah VP, Skelly JP, Amidon GL. Drug dissolution into micellar solutions: development of a convective diffusion model and comparison to the film equilibrium model with application to surfactant-facilitated dissolution of carbamazepine. *J Pharm Sci*. 1996;85(9):1005-1011.
- Crisp MT, Tucker CJ, Rogers TL, Williams RO, Johnston KP. Turbidimetric measurement and prediction of dissolution rates of poorly soluble drug nanocrystals. *J Control Release*. 2007;117(3):351-359.
- Hintz RJ, Johnson KC. The effect of particle-size distribution on dissolution rate and oral absorption. *Int J Pharm*. 1989;51(1):9-17.
- Kabalnov AS. Can micelles mediate a mass transfer between oil droplets? *Langmuir*. 1994;10:680-684.
- Lindfors L, Jonsson M, Weibull E, Brasseur JG, Abrahamsson B. Hydrodynamic effects on drug dissolution and deaggregation in the small intestine—a study with felodipine as a model drug. *J Pharm Sci*. 2015;104(9):2969-2976.
- Naylor LJ, Bakatselou V, Dressman JB. Comparison of the mechanism of dissolution of hydrocortisone in simple and mixed micelle systems. *Pharm Res*. 1993;10(6):865-870.
- Okazaki A, Mano T, Sugano K. Theoretical dissolution model of polydisperse drug particles in biorelevant media. *J Pharm Sci*. 2008;97(5):1843-1852.
- Rao VM, Lin MF, Larive CK, Southard MZ. A mechanistic study of griseofulvin dissolution into surfactant solutions under laminar flow conditions. *J Pharm Sci*. 1997;86(10):1132-1137.
- Shaeiwitz JA, Chan AFC, Cussler EL, Evans DF. The mechanism of solubilization in detergent solutions. *J Colloid Interf Sci*. 1981;84(1):47-56.
- Sugano K. Theoretical comparison of hydrodynamic diffusion layer models used for dissolution simulation in drug discovery and development. *Int J Pharm*. 2008;363(1-2):73-77.
- Sugano K. Aqueous boundary layers related to oral absorption of a drug: from dissolution of a drug to carrier mediated transport and intestinal wall metabolism. *Mol Pharm*. 2010;7(5):1362-1373.
- Sun W, Larive CK, Southard MZ. A mechanistic study of danazol dissolution in ionic surfactant solutions. *J Pharm Sci*. 2003;92(2):424-435.
- Wang YX, Abrahamsson B, Lindfors L, Brasseur JG. Comparison and analysis of theoretical models for diffusion-controlled dissolution. *Mol Pharm*. 2012;9(5):1052-1066.
- Wang YX, Abrahamsson B, Lindfors L, Brasseur JG. Analysis of diffusion-controlled dissolution from polydisperse collections of drug particles with an assessed mathematical model. *J Pharm Sci*. 2015;104(9):2998-3017.
- Johnson KC, Swindell AC. Guidance in the setting of drug particle size specifications to minimize variability in absorption. *Pharm Res*. 1996;13(12):1795-1798.
- Sugano K. Estimation of effective intestinal membrane permeability considering bile micelle solubilisation. *Int J Pharm*. 2009;368(1-2):116-122.
- Brunner E. Reaktionsgeschwindigkeit in heterogenen systemen. *Z Phys Chem*. 1904;47:56-102.
- Nernst W. Theorie der Reaktionsgeschwindigkeit in Heterogenen Systemen. *Z Phys Chem*. 1904;47:52-55.
- Almukainzi M, Okumu A, Wei H, Lobenberg R. Simulation of in vitro dissolution behavior using DDDPlus™. *AAPS PharmSciTech*. 2015;16(1):217-221.
- Ariyaprakai S, Dungan SR. Solubilization in monodisperse emulsions. *J Colloid Interf Sci*. 2007;314(2):673-682.
- Ariyaprakai S, Dungan SR. Contribution of molecular pathways in the micellar solubilization of monodisperse emulsion droplets. *Langmuir*. 2008;24(7):3061-3069.
- Dungan SR, Tai BH, Gerhardt NI. Transport mechanisms in the micellar solubilization of alkanes in oil-in-water emulsions. *Colloids Surf A*. 2003;216(1-3):149-166.
- Shekunov B. Theoretical analysis of drug dissolution in micellar media. *J Pharm Sci*. 2017;106:248-257.
- Harmon P, Galipeau K, Xu W, Brown C, Wuelfing WP. Mechanism of dissolution-induced nanoparticle formation from a copovidone-based amorphous solid dispersion. *Mol Pharm*. 2016;13(5):1467-1481.
- Fuguet E, Rafols C, Roses M, Bosch E. Critical micelle concentration of surfactants in aqueous buffered and unbuffered systems. *Anal Chim Acta*. 2005;548(1-2):95-100.
- Carey MC, Small DM. Micellar properties of dihydroxy and trihydroxy bile salts: effects of counterion and temperature. *J Colloid Interface Sci*. 1969;31:382-396.
- Peeters J, Neeskens P, Tollenaere JP, Van Remoortere P, Brewster ME. Characterization of the interaction of 2-hydroxypropyl-beta-cyclodextrin with itraconazole at pH 2, 4, and 7. *J Pharm Sci*. 2002;91(6):1414-1422.
- Jung JY, Yoo SD, Lee SH, Kim KH, Yoon DS, Lee KH. Enhanced solubility and dissolution rate of itraconazole by a solid dispersion technique. *Int J Pharm*. 1999;187(2):209-218.
- Duplatre G, Ferreira Marques MF, da Graca Miguel M. Size of sodium dodecyl sulfate micelles in aqueous solutions as studied by positron annihilation lifetime spectroscopy. *J Phys Chem*. 1996;100:16608-16612.
- Chen JM, Su TM, Mou CY. Size of sodium dodecyl-sulfate micelle in concentrated salt-solutions. *J Phys Chem*. 1986;90(11):2418-2421.
- Biorelevant homepage. Available at: <http://biorelevant.com>. Accessed November 1, 2016.
- Galia E, Nicolaidis E, Horter D, Lobenberg R, Reppas C, Dressman JB. Evaluation of various dissolution media for predicting in vivo performance of class I and II drugs. *Pharm Res*. 1998;15(5):698-705.
- Small DM. Phase equilibria and structure of dry and hydrated egg lecithin. *J Lipid Res*. 1967;8:551-557.
- Mazer NA, Benedek GB, Carey MC. Quasi-elastic light-scattering-studies of aqueous biliary lipid systems—mixed micelle formation in bile-salt lecithin solutions. *Biochemistry*. 1980;19(4):601-615.
- Meyerhoffer SM, McGown LB. Critical micelle concentration behavior of sodium taurocholate in water. *Langmuir*. 1990;6(1):187-191.
- Rabinow BE. Nanosuspensions in drug delivery. *Nat Rev*. 2004;3(9):785-796.
- Jacobs C, Kayser O, Muller RH. Production and characterisation of mucoadhesive nanosuspensions for the formulation of bupravaquone. *Int J Pharm*. 2001;214(1-2):3-7.
- Jounela AJ, Pentikainen PJ, Sothmann A. Effect of particle size on the bioavailability of digoxin. *Eur J Clin Pharmacol*. 1975;8(5):365-370.
- Junemann D, Dressman J. Analytical methods for dissolution testing of nanosized drugs. *J Pharm Pharmacol*. 2012;64(7):931-943.
- Kesisoglou F, Panmai S, Wu Y. Nanosizing—oral formulation development and biopharmaceutical evaluation. *Adv Drug Deliv Rev*. 2007;59(7):631-644.
- Muller RH, Jacobs C, Kayser O. Nanosuspensions as particulate drug formulations in therapy Rationale for development and what we can expect for the future. *Adv Drug Deliv Rev*. 2001;47(1):3-19.
- Muller RH, Keck CM. Challenges and solutions for the delivery of biotech drugs—a review of drug nanocrystal technology and lipid nanoparticles. *J Biotechnol*. 2004;113(1-3):151-170.
- Higuchi WI, Hiestand EN. Dissolution rates of finely divided drug powders. I. Effect of the distribution of particle sizes in a diffusion-controlled process. *J Pharm Sci*. 1963;52:67-71.
- Higuchi WI, Rowe EL, Hiestand EN. Dissolution rates of finely divided drug powders. II. Micronized methyl-prednisolone. *J Pharm Sci*. 1963;52:162-164.
- Sheng JJ, Sirois PJ, Dressman JB, Amidon GL. Particle diffusional layer thickness in a USP dissolution apparatus II: a combined function of particle size and paddle speed. *J Pharm Sci*. 2008;97(11):4815-4829.
- Galli C. Experimental determination of the diffusion boundary layer width of micron and submicron particles. *Int J Pharm*. 2006;313(1-2):114-122.
- Amidon GL, Lennernas H, Shah VP, Crison JR. A theoretical basis for a biopharmaceutic drug classification: the correlation of in vitro drug product dissolution and in vivo bioavailability. *Pharm Res*. 1995;12(3):413-420.